Angelov, B.; Haramus, V.M.; Drechsler, M.; Angelova, A.:

Structural analysis of nanoparticulate carriers for encapsulation of macromolecular drugs

In: Journal of Molecular Liquids (2016) Elsevier

DOI: 10.1016/j.molliq.2016.11.064

Structural Analysis of Nanoparticulate Carriers for Encapsulation of Macromolecular Drugs

Borislav Angelov[a], Vasil M. Garamus[b,*], Markus Drechsler[c], Angelina Angelova[d]

[a]Institute of Physics, ELI Beamlines, Academy of Sciences of the Czech Republic, Na Slovance 2, CZ-18221 Prague, Czech Republic,

[b]Helmholtz-Zentrum Geesthacht: Centre for Materials and Coastal Research, D-21502 Geesthacht, Germany ,

[c]Laboratory for Soft Matter Electron Microscopy, Bayreuth Institute of Macromolecular Research, University of Bayreuth, D-95440 Bayreuth,

[d]Institut Galien Paris-Sud, CNRS UMR 8612, Univ. Paris-Sud, Université Paris-Saclay, LabEx LERMIT, F-92290 Châtenay-Malabry cedex, France

* Corresponding author: Vasyl.Haramus@hzg.de

Highlights

- Liquid dispersions of cationic lipids for pDNA (BDNF) delivery characterized by SAXS
- Structural phase transitions occur upon compaction of pDNA in cationic lipid nanocarriers
- Hexosome particles, inverted hexagonal phases, and onion-type complexes formed
- Cationic lipid structure tunes the supramolecular organization of the gene carriers

Abstract

Recently developed macromolecular drugs display strong potential to cure diseases involving genetic components, *e.g*. Rheumatoid arthritis, diabetes, Alzheimer's disease, Huntington's disease, Duchenne muscular dystrophy, Retinitis pigmentosa, and several types of cancers. Bioavailability and enhanced drug specificity necessitate the preparation of efficient carrier systems for the macromolecular therapeutics. We employ synchrotron small-angle X-ray scattering (SAXS) and cryogenic transmission electron microscopy (Cryo-TEM) to study the nanostructure formation, macromolecular drug upload, and the topological transformations occurring upon complexation of supercoiled plasmid DNA (encoding for the therapeutic protein brain-derived neurotrophic factor, BDNF) with cationic lipid nanocarrier assemblies. Understanding of the liquid crystalline nanostructure formation (hexosomes, cubosomes, inverted hexagonal and intermediate mesophases, or onion-type complexes) enabling efficient delivery of new generation sequencing systems is expected to contribute to the progress in precision nanomedicine and the treatment of various severe diseases.

Graphical abstract

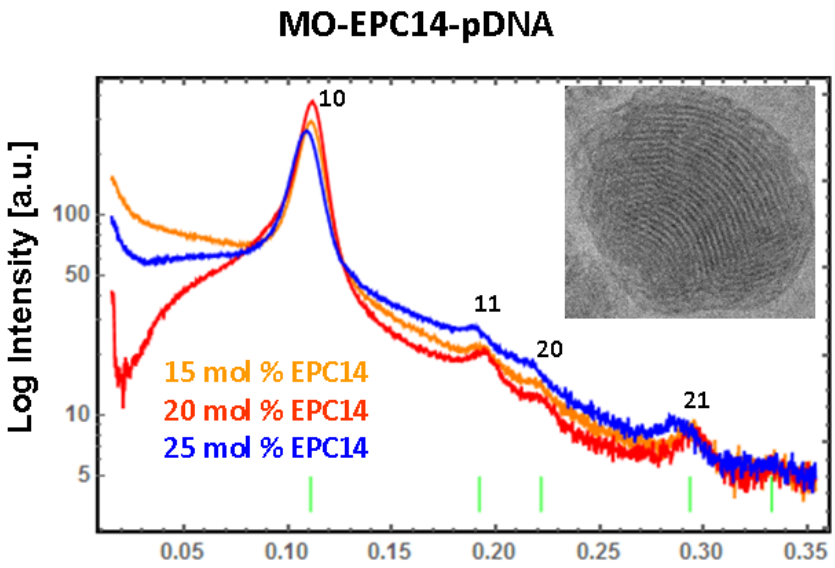

BioSAXS patterns evidence the structural phase transformations occurring upon uptake and complexation of supercoiled plasmid DNA (pBDNF) in cationic lipid nanocarriers

Keywords

- self-assembled nanocarriers,
- liquid crystalline phase transitions,
- cationic lipids,
- macromolecular drugs,
- CRISPR/Cas9 therapeutics,
- synchrotron SAXS

1. Introduction

Macromolecular therapeutics (recombinant proteins, antibodies, synthetic peptides, oligonucleotides, and cell penetrating peptide-drug conjugates) have gained considerable recent interest owing to their success rate in clinical development as compared to conventional small organic molecule drugs [1]. There has been evidence that tumor-selective delivery of macromolecular therapeutics may be highly efficient in curing the pathological states [2-4]. Therefore, nanocarrier systems enhancing the bioavailability of the macromolecular drugs through encapsulation and slow release or PEGylation (*i.e.* conjugation with polyethylene glycol chains) are under current development [5-18].

Modern directions in precision nanomedicine account for the fact that severe diseases such as cancers often involve DNA mutations, gene duplications, and changes in messenger RNAs [19,20]. Importantly, next-generation sequencing technologies have a potential to correct the mutations causing the pathologies with genetic components, for instance in diabetes, Rheumatoid arthritis, cancers (breast, lung, and thyroid cancer), Alzheimer's disease, Huntington's disease, Duchenne muscular dystrophy, and Retinitis pigmentosa [19-25]. New perspectives further to recombinant proteins, siRNA (small interfering RNAs, a class of double-stranded RNA molecules, 20-25 base pairs in length) and monoclonal antibodies, have emerged based on the CRISPR/Cas9 technology for genome editing [20,22]. The CRISPR/Cas9 therapeutics [Clustered Regularly Interspaced Short Palindromic Sequences (CRISPRs) associated with a programmable genome-editing enzyme *Cas9* endonuclease] have shown promise for correction of single or multiple gene mutations based on advanced genome editing technology [20]. Multiple target gene sequences can be simultaneously edited by adding more than one guide RNA (gRNAs) in a single transfection reaction.

It should be stressed that multiplex genome editing in CRISPR/Cas9-mediated therapies using all-in-one vector to knock-out, repress or activate target genes will need to resolve key issues of macromolecular drug transport and delivery [25-32]. Plasmids of the CRISPR/Cas9 category of macromolecular drugs are very large constructs and do not cross the biological barriers. Therefore, the safety and the performance of the delivery systems of CRISPR/Cas9 therapeutics should be improved in order to achieve their uniform and sustained administration into the cells. The large biomacromolecules need to be compacted for entry into the cells *via* carriers [33-39]. The negative charge of the nucleic acids imposes obstacles for their interaction and passage across the cell membranes [40-44].

Cationic lipid-mediated delivery of proteins and therapeutic genetic material into cells may be ensured by liquid crystalline type nanocarriers as nonviral vectors [45-56]. The role of the lipid type for the complexation of macromolecular plasmid DNA (pDNA) or siRNA therapeutics with positively charged nanocarriers has gain considerable attention towards the

aim of improving their transfection efficiency [18,45,47,53,54]. It has been reported that mesophase transformations of the nanocarriers may be influenced by the geometry of the lipid/water interfaces, and their charge and hydration [12,13,38,53,54]. In this research, structural methods including small-angle neutron and X-ray scattering have been indispensable for determination of the mesophase transitions and the organization of the nanostructured liquids that provide efficient particle internalization into cells [56-60]. It has been shown that compaction of the charged macromolecular drugs may be achieved within inverted hexagonal, multilamellar, onion or cubic membrane type lipid carriers [52,53]. An important advantage of self-assembled lipid carriers is that inverted hexagonal and inverted cubic membrane architectures provide multicompartment nanochannel organization for protection and control release of the macromolecular therapeutics [6,7,51-56].

The purpose of the present study is to investigate the self-assembled structures formed by mixtures of two kinds of cationic lipids and a nonlamellar helper lipid in nanocarriers for complexation and compaction of macromolecular therapeutic agents. The compaction and uptake of a model plasmid encoding for the therapeutic protein brain-derived neurotrophic factor (BDNF) is investigated by synchrotron small-angle X-ray scattering (SAXS) and cryogenic transmission electron microscopy (Cryo-TEM) in aqueous dispersions of cationic lipid nanoparticles. The attachment of polyethylene glycol (PEG) chains to the nanoparticle surfaces, through inclusion of PEGylated lipids at the lipid/water interfaces, provided steric stabilization of the studied formulations.

2. Materials and methods

2.1. Materials and sample preparation

The cationic lipid *1,2*-dimyristoly-*sn*-glycero-*3*-ethylphosphocholine (EPC14) (M_w=742.45 g/mol) and the PEGylated lipid *1,2*-dioleoyl-*sn*-glycero-*3*-phosphoethanolamine-*N*-(methoxy (polyethyleneglycol)-2000) ammonium salt (DOPE-PEG_{2000}) (M_W 2801.51 g/mol) were products of *Avanti Polar Lipids* and purchased by *Coger* (Paris). The neutral monoglyceride lipid monoolein (MO) was used as a helper lipid (1-oleoyl-*rac*-glycerol, M_W 356.55 g/mol, purity 99.5%, *Sigma*). The cationic amphiphile hexadecyltrimethylammonium bromide (CTAB) (M_W 364.46, BioUltra, ≥99.0%, *Fluka*) was used as received from *Sigma*. Phosphate buffer solution (NaH_2PO_4/Na_2HPO_4, 1.10^{-2}M, pH 7, p.a. grade, *Merck*) was prepared using Milli-Q water (*Millipore Co.*). Aqueous dispersions of liquid crystalline particles were prepared at ambient temperature by hydration of a lyophilized mixed lipid film, multiple vortex shakings, and agitation by sonication. The organic solvent chloroform was evaporated under flux of nitrogen gas. An ultrasonication ice bath (Branson 2510 ultrasonic bath, "set sonics" mode) was periodically applied during 2-4 minutes in order to get

homogeneous liquid dispersions of cationic nanoparticles. Homogeneous dispersion of the EPC14-containing samples required addition of ice to the sonication bath in order to keep low temperature environment. Endotoxin-free plasmid DNA (pBDNF), encoding for human BDNF (brain-derived neurotrophic factor), was prepared by custom gene synthesis, subcloning and purification (*GenScript Co*.).

2.2. SAXS measurements

Synchrotron SAXS experiments were performed at the P12 BioSAXS beamline of the European Molecular Biology Laboratory (EMBL) at the storage ring PETRA III of the Deutsche Elektronen Synchrotron (DESY, Hamburg, Germany) at 20 °C using a Pilatus 2M detector (1475 x 1679 pixels) (Dectris, Switzerland) and synchrotron radiation with a wavelength λ = 1 Å. The sample-to-detector distance was 3 m, allowing for measurements in the *q*-range interval from 0.01 to 0.44 $Å^{-1}$. The *q*-vector was defined as $q = (4\pi/\lambda) \sin \theta$, where 2θ is the scattering angle. The *q*-range was calibrated using the diffraction patterns of silver behenate. The experimental data were normalized with respect to the transmitted beam intensity. The background scattering of the quartz capillary and aqueous buffer was subtracted. The aqueous buffer scattering was measured before and after every sample scattering in order to control for eventual sample holder contamination. Twenty consecutive frames (each 0.05s) comprising the measurements for the sample and the solvent were acquired. No measurable radiation damage was detected by the comparison of frames. An automatic sample changer adjusted for sample volume of 20 μL and a filling cycle of 1 min was used.

2.3. Cryogenic Transmission Electron Microscopy (Cryo-TEM)

For cryo-TEM studies, a sample droplet of 2 μL was put on a lacey carbon film covered copper grid (Science Services, Munich, Germany), which was hydrophilized by glow discharge for 15 s. Most of the liquid was then removed with blotting paper, leaving a thin film stretched over the lace holes. The specimens were instantly shock frozen by rapid immersion into liquid ethane and cooled to approximately 90 K by liquid nitrogen in a temperature-controlled freezing unit (Zeiss Cryobox, Zeiss NTS GmbH, Oberkochen, Germany). The temperature was monitored and kept constant in the chamber during all the sample preparation steps. After the specimens were frozen, the remaining ethane was removed using blotting paper. The specimen was inserted into a cryo transfer holder (CT3500, Gatan, Munich, Germany) and transferred to a Zeiss EM922 Omega energy-filtered TEM (EFTEM) instrument (Zeiss NTS GmbH, Oberkochen, Germany). Examinations were carried out at temperatures around 90 K. The TEM instrument was operated at an acceleration voltage of 200 kV. Zero-loss-filtered images (ΔE = 0 eV) were taken under reduced dose conditions (100-1000 e/nm^2). The images were recorded digitally by a bottom-mounted charge-coupled device (CCD) camera system (Ultra Scan 1000, Gatan, Munich, Germany) and combined and processed with a digital imaging processing system (Digital Micrograph GMS 1.8, Gatan,

Munich, Germany). The sizes of the investigated nanoparticles were in the range or below the film thickness and no deformations were observed. The images were taken very close to focus or slightly under the focus (some nanometers) due to the contrast enhancing capabilities of the in-column filter of the used Zeiss EM922 Omega. In EFTEMs, deep underfocused images can be totally avoided.

3. Results and discussion

3.1. Self-assembled nanopaticulate carriers formed by cationic and monoglyceride amphiphiles

The principles applicable to self-assembly of cationic lipid carriers with therapeutic macromolecules suitable for genetic modifications are applied here to demonstrate the power of the structural BioSAXS measurements, performed at synchrotron radiation facility, for determination of the nanostructures generated in diluted liquid formulations. The patterns of blank nanocarriers self-assembled from the nonlamellar lipid monoolein (MO) (helper lipid) upon inclusion of different molar percentages of a double chain 1,2-dimyristoly-*sn*-glycero-*3*-ethylphosphocholine (EPC14) lipid or a single chain hexadecyltrimethylammonium bromide (CTAB) cationic component are presented in Fig. 1a and 2a, respectively. The molar content of the positively charged lipids (EPC14 and CTAB) was varied as 15, 20 and 25 mol% with regard to the nonlamellar helper lipid MO. The nanocarriers were sterically stabilized by the lipopolymer DOPE-PEG_{2000}.

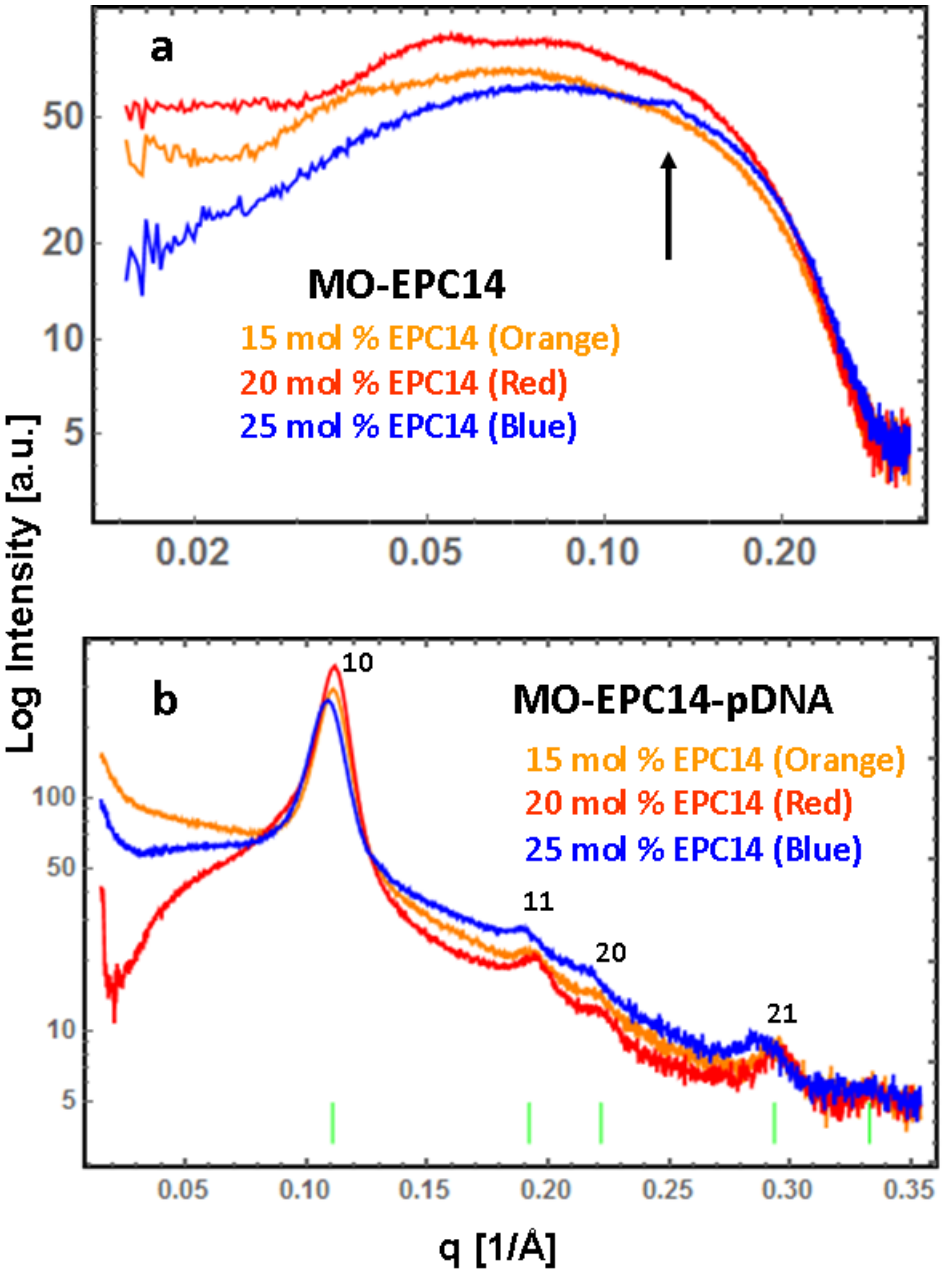

Figure 1

Figure 1. Synchrotron SAXS patterns of aqueous dispersions of self-assembled lipid MO/EPC14/DOPE-PEG_{2000} carriers at varying molar percentages of the cationic component (15, 20 and 25 mol% EPC14) before (a) and after uptake and complexation (b) with plasmid DNA (pBDNF). The concentration of the PEGylated lipid DOPE-PEG_{2000} in the mixed assemblies was kept constant (3 mol%). The arrow in (a) indicates the position of a weak peak of an inverted hexagonal structure. The Bragg peaks of an inverted hexagonal lattice are indexed in (b).

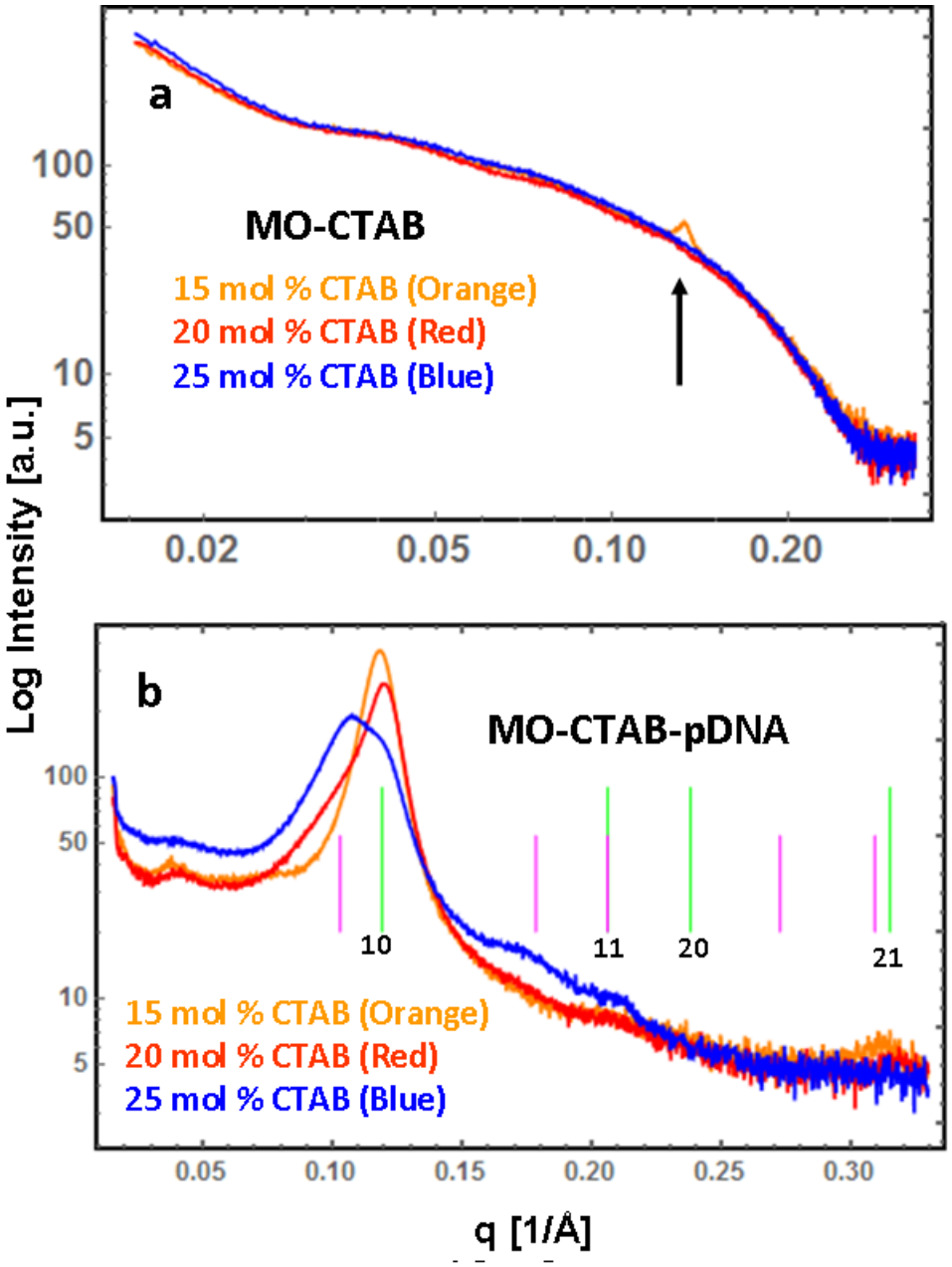

Figure 2. Synchrotron SAXS patterns of aqueous dispersions of self-assembled lipid MO/CTAB/DOPE-PEG$_{2000}$ carriers at varying molar percentages of cationic component (15, 20 and 25 mol% CTAB) before (a) and after uptake and complexation (b) with plasmid DNA (pBDNF). The concentration of the PEGylated lipid DOPE-PEG$_{2000}$ in the mixed assemblies was kept constant (2 mol%). The arrow in (a) indicates the position of a weak peak of an inverted hexagonal structure. The Bragg peaks of two coexisting inverted hexagonal structures are indexed in (b).

Figures 1a and 2a show that the major nanoparticles population in the MO/EPC14/DOPE-PEG_{2000} and MO/CTAB/DOPE-PEG_{2000} dispersions contains vesicular membrane type nanocarriers and precursors of small cubosomes. Scattering curves of such shapes have been previously observed for aqueous dispersions of PEGylated particles derived from the nonlamellar lipid monoolein and PEGylated lipids [30]. A minor fraction of the nanoparticle populations appears to form precursors of hexosome carriers, which display a weak peak of an inverted hexagonal structure (see the arrows at a scattering vector q ~0.13 Å in Figures 1a and 2a). The SAXS plots recorded at varying molar percentages of cationic lipids indicate that the formation of hexosome assemblies is favoured at the highest molar fraction of the double chain cationic lipid EPC14 (Fig. 1a) and at the lowest molar fraction of the single chain cationic amphiphile CTAB (Fig. 2a). The corresponding lattice parameter of the H_{II} structures is around 65 Å. It may be suggested that the hexosome formation might be due to the capacity of the EPC14 headgroups to reduce the hydration of the monoolein lipid membrane interfaces, which is associated with increase in the interfacial curvature and a possible nonlamellar cubic-to-inverted hexagonal phase transition.

3.2. Structural transitions upon macromolecular drug uptake and compaction in nanocarriers

Cationic lipid/pDNA(BDNF) nanocomplexes were assembled after dilution of the stock pDNA solution in a phosphate buffer and subsequent incubation with dispersions of cationic lipid MO/EPC14/DOPE-PEG_{2000} or MO/CTAB/DOPE-PEG_{2000} nanocarriers. The complexation reaction is driven by electrostatic interactions between the positively charged nanoparticles and the negatively charged pDNA macromolecules. The concentration of the positive charges in the lipid nanoparticle systems was varied through the EPC/MO and CTAB/MO molar ratios, while keeping same pDNA(BDNF) solution concentration. In fact, the negative charges of pDNA were maintained in deficiency with respect to the available cationic charges in the reaction volume in order to avoid the overall precipitation of the generated pDNA/lipid complexes. The formation of lipoplexes between the macromolecular pDNA (BDNF) with the cationic EPC14- and CTAB-containing nanoparticle dispersions was investigated at a constant content of the helper lipid MO and the PEGylated lipid DOPE-PEG_{2000}.

The ultrastructures occurring upon complexation of the macromolecular drug pDNA(BDNF) with the two types of cationic lipid carriers were determined by SAXS (Fig. 1b and Fig. 2b). At variance to previous reports on pDNA compaction by cationic lipids, we did not observe multilamellar sandwich-type lipoplex formation that is typical for pDNA intercalation in stacked lipid bilayer membranes. Figures 1b and 2b clearly show that the complexation of pDNA(BDNF) within the studied cationic lipid carriers leads to a structural

transformation of the vesicular membranes into MO-EPC14-pDNA and MO-CTAB-pDNA lipoplexes of nonlamellar-type supramolecular organizations. pDNA uptake and insertion into the cationic lipid particles give raise to strong Bragg peaks indicative for the induction of inverted hexagonal phase structures.

Four orders of Bragg peaks (10), (11), (20), and (21) of an inverted hexagonal lattice were indexed in Fig. 1b. They determine lattice parameters, a_{HII}, for the pDNA/MO/EPC14/DOPE-PEG_{2000} assemblies in the range of 65-66 Å. One observes a slight shift of the Bragg peak as a function of the cationic lipid molar percentage, namely a_{HII} = 65.2 Å at 15 mol% and 20 mol% of EPC14 (orange and red plots in Fig. 1b) and a_{HII} = 65.9 Å at 25 mol% EPC14 (blue plot in Fig. 1b). This suggests tuning of the degree of macromolecular pDNA compaction upon its uptake into lipid nanocarriers of varying positive charges.

The SAXS results in Figure 2b revealed more sophisticated patterns for the dispersed pDNA/MO/CTAB/DOPE-PEG_{2000} assemblies. Bragg peaks of two coexisting inverted hexagonal structures were indexed. The lattice parameter of the first H_{II} structure was determined as a_{HII} = 60.9 Å, whereas the second structure was characterized by a_{HII} = 70.4 Å. In addition, cubosomal precursors with internal liquid crystalline structure were observed at low *q* values, which might correspond to blank carriers with no entrapped pDNA. Evidently, the excess positive charges (which are not compensated by pDNA binding) favour the formation of coexisting hexosome structures with a bigger H_{II} lattice (a_{HII} = 70.4 Å) and larger aqueous channels.

The above SAXS results suggest that the homogeneity and the pDNA entrapment efficiency of the MO/EPC14/DOPE-PEG_{2000} cationic nanoparticulate system appear to be higher than that of the MO/CTAB/DOPE-PEG_{2000} carriers. The two kind of cationic lipid carriers provide different charge neutralization capacity of the lipid/water interfaces for binding of the multivalent ions of the pDNA. Figure 3 shows a comparison of the SAXS plots of the blank and pDNA-loaded carriers for the two types of cationic lipids at a constant positive charge of 20 mol% cationic agent in the self-assembled mixtures. At same molar percentage of positive charges, the cationic lipid structures lead to differences in the stabilization of the formed lipoplexes. The established different degree of compaction of the macromolecular drug pDNA by the double-chain EPC14 or the single-chain CTAB cationic lipid agents may require further investigations by spectroscopic methods.

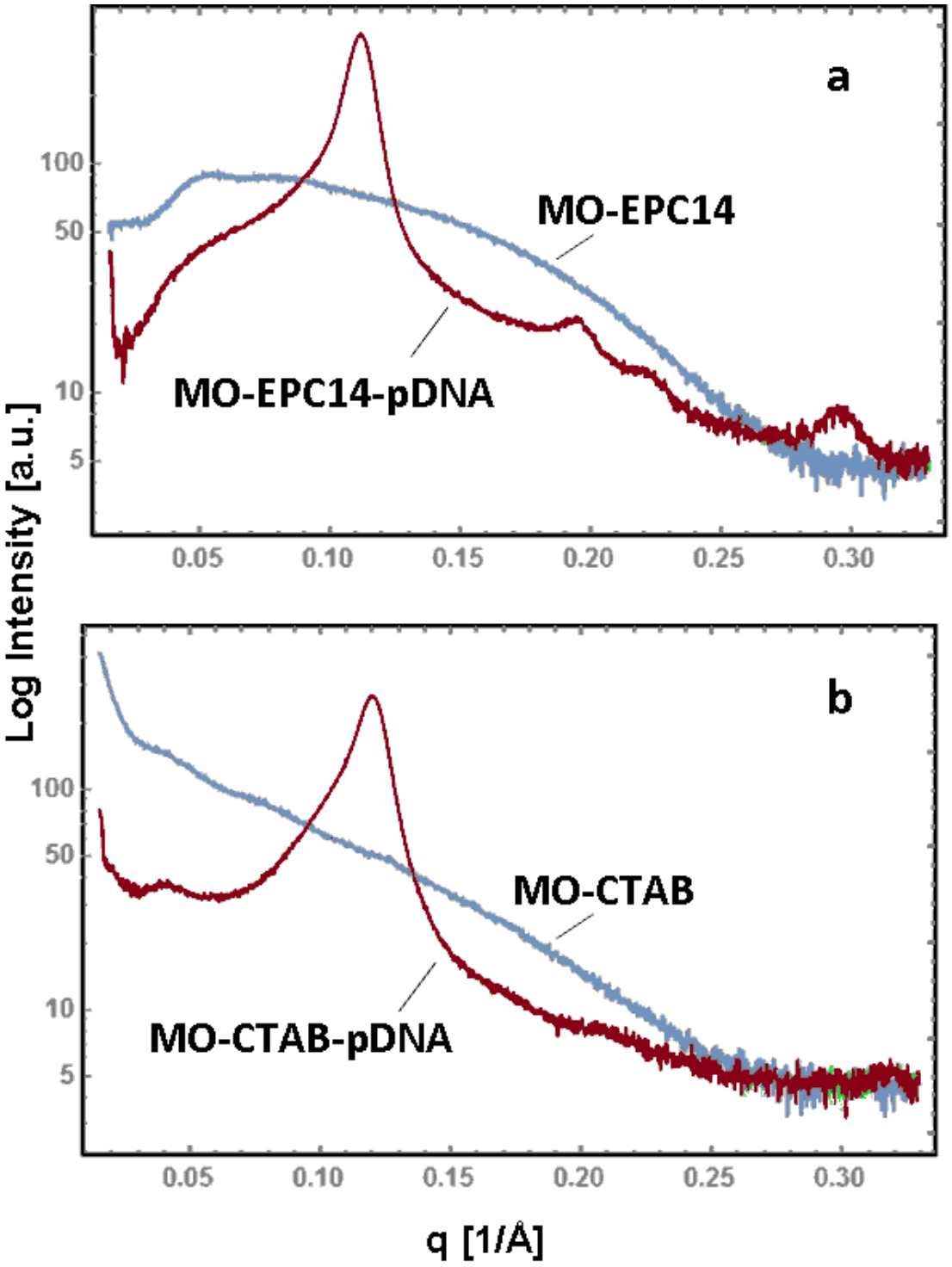

Figure 3. Comparison of SAXS patterns of MO/EPC14/DOPE-PEG_{2000} and MO/CTAB/DOPE-PEG_{2000} nanocarriers and of the corresponding lipoplexes with pDNA (MO-EPC14-pDNA and MO-CTAB-pDNA) formed at constant positive charge (20 mol% cationic lipid content). The concentration of the DOPE-PEG_{2000} lipid in the mixed assemblies is 3 mol% in the case of EPC-containing carriers (a) and 2 mol% for CTAB-containing nanocarriers (b).

3.3. Morphological structural transition upon lipoplex formation with monoolein/cationic lipid nanoparticles

The performed microscopy study by cryo-TEM evidenced the structural transformations upon pDNA binding and uptake in the selected self-assembled lipid nanoparticles. Figure 4 presents cryo-TEM images demonstrating different stages of the structural transition from pDNA-decorated bilayer membranes vesicles to hexosomes and inverted hexagonal type nanocarriers. The initial self-assembled nanostructures of onion type organization are transformed into more densely packed assemblies of inverted hexagonal packing. The small number of lamellas in the lipid particles (Fig. 4 (a,b)) undergo a phase transition through intermediate stages (Fig. 4 (c,d)) in order to reach tubular organization of an inverted hexagonal type liquid crystalline structure (Fig. 4 (e)). It has been indicated that hexosomes and inverted hexagonal phases present more important structural advantages for efficient compaction and delivery of DNA therapeutics, and have been shown to be more efficient in gene transfection studied with regard to lamellar type DNA/lipid complexes [53,54].

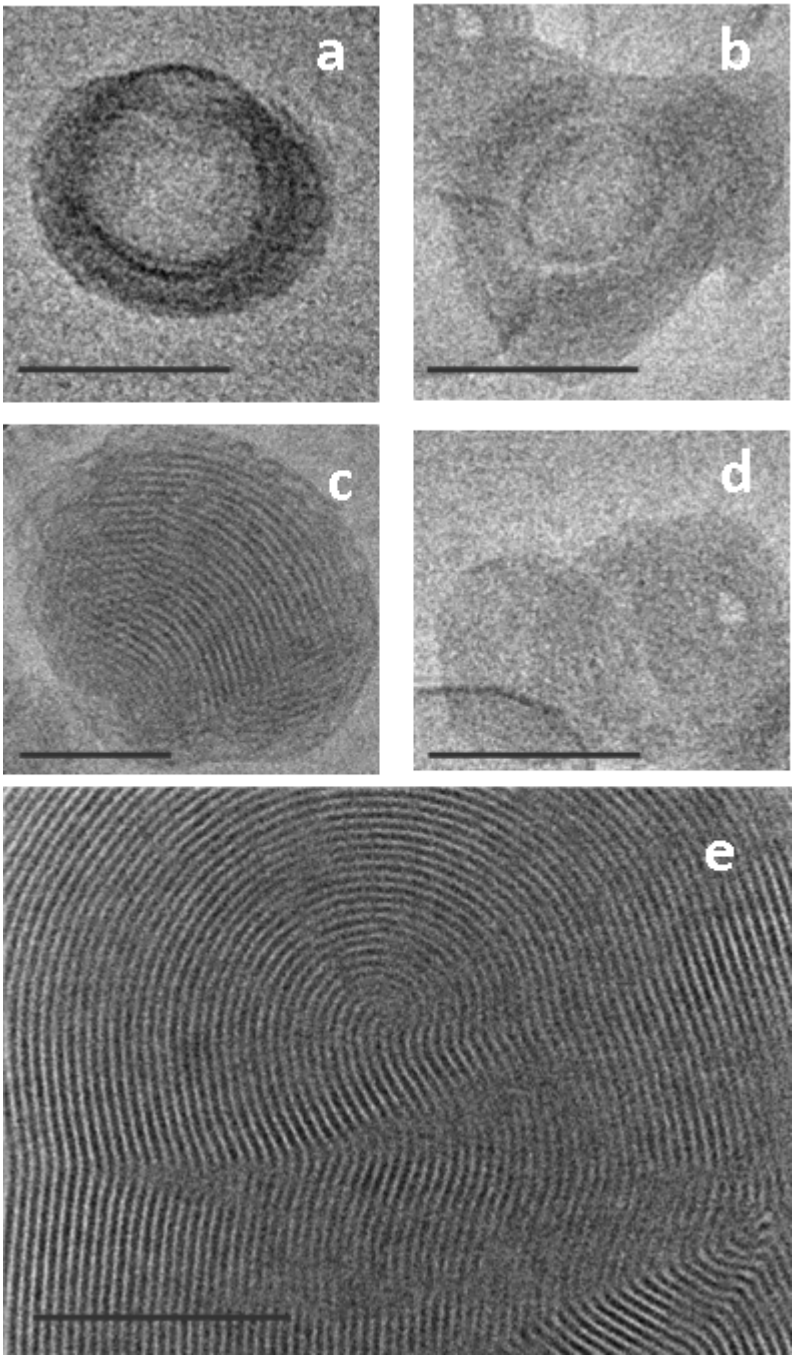

Figure 4. Cryogenic transmission electron microscopy (Cryo-TEM) images showing stages of formation of self-assembled lipoplex nanostructures of liquid crystalline organization: (a,b) nanoparticles with onion lamellar packing; (c,d) intermediates of inverted hexagonal packing, and (e) hexosome carriers with long range order of inverted hexagonal structure. The bar corresponds to 100 nm.

4. Conclusions

Determination of the structural features of supramolecular assembly and complexation between fusogenic lipid nanoparticles of nanochannelled organization, *e.g*. monoolein-based cationic cubosome nanoparticles, with plasmid DNA encoding for the therapeutic protein BDNF is of current interest for the development of anti-Alzheimer's therapeutic approaches [57]. Mixed amphiphilic assemblies, involving the cubic-phase forming lipid monoolein and two types of cationic lipids (double chain EPC14 and single chain CTAB), were studied for generation of delivery vehicles of pDNA (neurotrophin BDNF). The advantage of the cubic-phase forming lipids for gene transfer is that they may provoke, *via* interfacial curvature variations, substantial structural effects on the cell membrane barriers [58]. Therefore, they may serve for the creation of fusogenic nanocarriers for controlled drug release. The obtained here liquid dispersions of cationic lipids for pDNA (BDNF) delivery were characterized by synchrotron BioSAXS. A coexistence of multiple types of dispersed lipid particles and lipoplexes was established. Hexosome particles and inverted hexagonal phases were formed upon progression of the complexation process starting from onion-type nanocarriers. The BioSAXS data indicated that the cationic lipid structure tunes the supramolecular organization of the gene carriers. Structural phase transitions occurred upon uptake and compaction of pDNA into lipid nanocarriers of an inverted hexagonal type. These results provide further advances to the field of amphiphile nanoarchitectonics and soft matter nanostructures for drug delivery [59-73].

Acknowledgement

We gratefully acknowledge the allocation of beam time at the Synchrotron Radiation Facility DESY (Deutsche Elektronen Synchrotron, Hamburg, Germany) – storage ring PETRA III, BioSAXS beamline P12 of the European Molecular Biology Laboratory (EMBL). B.A. was supported by the project ELI - Extreme Light Infrastructure – phase 2 (CZ.02.1.01/0.0/0.0/15_008/0000162) from European Regional Development Fund. M.D. thanks BIMF (Bayreuth Institute of Macromolecular Research) and BZKG (Bayreuth Center for Colloids and Interfaces) for financial support.

References

[1] M. Hay, D.W. Thomas, J.L. Craighead, C. Economides, J. Rosenthal, Clinical development success rates for investigational drugs, Nat. Biotechnol., 32 (2014) 40-51.

[2] T.M. Allen, P.R. Cullis, Liposomal drug delivery systems: From concept to clinical applications, Adv. Drug Delivery Reviews, 65 (2013) 36-48.

[3] H. Maeda, Tumor-selective delivery of macromolecular drugs via the EPR effect: Background and future prospects, Bioconjugate Chem., 21 (2010) 797–802.

[4] V. Torchilin, Tumor delivery of macromolecular drugs based on the EPR effect. Adv. Drug Delivery Reviews, 63 (2011) 131–135.

[5] B. Ying, R.B. Campbell, Delivery of kinesin spindle protein targeting siRNA in solid lipid nanoparticles to cellular models of tumor vasculature, Biochemical and Biophysical Research Communications, 446 (2014) 441-447.

[6] A. Angelova, B. Angelov, M. Drechsler, V.M. Garamus, S. Lesieur, Protein entrapment in PEGylated lipid nanoparticles. Int. J. Pharm., 454 (2013) 625–632.

[7] B. Angelov, A. Angelova, S.K. Filippov, M. Drechsler, P. Štěpánek, S. Lesieur, Multicompartment lipid cubic nanoparticles with high protein upload: millisecond dynamics of formation. ACS Nano, 8 (2014) 5216–26.

[8] A. Angelova, B. Angelov, B. Papahadjopoulos-Sternberg, M. Ollivon, C. Bourgaux, Structural organization of proteocubosome carriers involving medium- and large-size proteins. J Drug Deliv Sci Tec., 15 (2005) 108–112.

[9] R. Negrini, R. Mezzenga, pH-responsive lyotropic liquid crystals for controlled drug delivery, Langmuir, 27 (2011) 5296-5303.

[10] S. Yu, C. He, J. Ding, Y. Cheng, W. Song, X. Zhuang, X. Chen, pH and reduction dual responsive polyurethane triblock copolymers for efficient intracellular drug delivery, Soft Matter, 9 (2013) 2637-2645.

[11] R. Negrini, R., Mezzenga, Diffusion, molecular separation, and drug delivery from lipid mesophases with tunable water channels, Langmuir, 28 (2012) 16455-16462.

[12] B. Angelov, A. Angelova, S.K. Filippov, T. Narayanan, M. Drechsler, P. Štěpánek, P. Couvreur, S. Lesieur, DNA/fusogenic lipid nanocarrier assembly: Millisecond structural dynamics. J Phys Chem Lett., 4 (2013) 1959-1964.

[13] B. Angelov, A. Angelova, S.K. Filippov, G. Karlsson, N. Terrill, S. Lesieur, P. Štěpánek, Topology and internal structure of PEGylated lipid nanocarriers for neuronal

transfection: Synchrotron radiation SAXS and cryo-TEM studies. Soft Matter, 7 (2011) 9714-9720.

[14] B. Angelov, A. Angelova, B. Papahadjopoulos-Sternberg, S. Lesieur, J.F. Sadoc, M. Ollivon, P. Couvreur, Detailed structure of diamond-type lipid cubic nanoparticles. J. Am. Chem. Soc., 128 (2006) 5813–5817.

[15] J. Croissant, X. Cattoën, M. Wong Chi Man, P. Dieudonné, C. Charnay, L. Raehm, J.O. Durand, One-pot construction of multipodal hybrid periodic mesoporous organosilica nanoparticles with crystal-like architectures, Advanced Materials, 27 (2015) 145-149.

[16] R. Chandrawati, M.P. Van Koeverden, H. Lomas, F. Caruso, Multicompartment particle assemblies for bioinspired encapsulated reactions, Journal of Physical Chemistry Letters, 2 (2011) 2639-2649.

[17] J.Y.T. Chong, X. Mulet, L.J. Waddington, B.J. Boyd, C.J. Drummond, High-throughput discovery of novel steric stabilizers for cubic lyotropic liquid crystal nanoparticle dispersions, Langmuir, 28 (2012) 9223-9232.

[18] N. Zeng, X. Gao, Q. Hu, Q. Song, H. Xia, Z. Liu, G. Gu, M. Jiang, Z. Pang, H. Chen, J. Chen, L. Fang, Lipid-based liquid crystalline nanoparticles as oral drug delivery vehicles for poorly water-soluble drugs: Cellular interaction and in vivo absorption, International Journal of Nanomedicine, 7 (2012) 3703-3718.

[19] A.G. Bassuk, A. Zheng Y. Li, S.H. Tsang, V.B. Mahajan, Precision medicine: genetic repair of retinitis pigmentosa in patient-derived stem cells. Scientific Reports, 6 (2016) 19969.

[20] S.S. Yadav, J. Li, H.J. Lavery, K.K. Yadav, A.K. Tewari, Next-generation sequencing technology in prostate cancer diagnosis, prognosis, and personalized treatment. Urol Oncol., 33 (2015) 267-313.

[21] W. Sun, W. Ji, J.M. Hall, Q. Hu, C. Wang, C.L. Beisel, Z. Gu, Self-assembled DNA nanoclews for the efficient delivery of CRISPR-Cas9 for genome editing. Angew. Chemie, 127 (2015) 12197-12201.

[22] S. Yao, Z. He, C. Chen, CRISPR/Cas9-mediated genome editing of epigenetic factors for cancer therapy. Human Gene Therapy, 26 (2015) 463-471.

[23] J.A. Zuris, D.B. Thompson, Y. Shu, J.P. Guilinger, J.L. Bessen, J.H. Hu, M.L. Maeder, J.K. Joung, Z.Y. Chen, D.R. Liu, Cationic lipid-mediated delivery of proteins enables efficient protein-based genome editing in vitro and in vivo. Nat Biotechnol., 33 (2015) 73-80.

[24] A.M. Kabadi, D.G. Ousterout, I.B. Hilton, C.A. Gersbach, Multiplex CRISPR/Cas9-based genome engineering from a single lentiviral vector. Nucleic Acids Res., 42 (2014) e147.

[25] S. Falsini, L. Ciani, S. Ristori, A. Fortunato, A. Arcangeli, Advances in lipid-based platforms for RNAi therapeutics. Journal of Medicinal Chemistry, 57 (2014) 1138-1146.

[26] P. Tam, M. Monck, D. Lee, O. Ludkovski, E.C. Leng, K. Clow, H. Stark, P. Scherrer, R.W. Graham, P.R. Cullis, Stabilized plasmid-lipid particles for systemic gene Therapy, Gene Therapy, 7 (2000) 1867-1874.

[27] C. Wan, T. M. Allen, P. R. Cullis, Lipid nanoparticle delivery systems for siRNA-based therapeutics. Drug Delivery and Translational Research, 4 (2014) 74-83.

[28] A.K. Leung, Y.Y. Tam, P. R. Cullis, Lipid nanoparticles for short interfering RNA delivery. Adv. Genet., 88 (2014) 71-110.

[29] B. Angelov, A. Angelova, V.M. Garamus, G. Le Bas, S. Lesieur, M. Ollivon, S.S. Funari, R. Willumeit, P. Couvreur, Small-angle neutron and X-ray scattering from amphiphilic stimuli-responsive diamond-type bicontinuous cubic phase. J. Am. Chem. Soc., 129 (2007) 13474−13479.

[30] B. Angelov, A. Angelova, V.M. Garamus, M. Drechsler, R. Willumeit, R. Mutafchieva, P. Štěpánek, S. Lesieur, Earliest stage of the tetrahedral nanochannel formation in cubosome particles from unilamellar nanovesicles. Langmuir, 28 (2012) 16647–16655.

[31] A. Yaghmur, M. Rappolt, J. Oøstergaard, C. Larsen, S.W. Larsen, Characterization of bupivacaine-loaded formulations based on liquid crystalline phases and microemulsions: The effect of lipid composition, Langmuir, 28 (2012) 2881-2889.

[32] G.C. Kuang, X.R. Jia, M.J. Teng, E.Q. Chen, W.S. Li, Y. Ji, Y., Organogels and liquid crystalline properties of amino acid-based dendrons: A systematic study on structure-property relationship, Chemistry of Materials, 24 (2012) 71-80.

[33] Y.S. Tarahovsky, Cell transfection by DNA-lipid complexes – lipoplexes. Biochemistry (Moscow), 74 (2009) 1293-1304.

[34] S. Huebner, B.J. Battersby, R. Grimm, G. Cevc, Lipid-DNA complex formation: reorganization and rupture of lipid vesicles in the presence of DNA as observed by cryoelectron microscopy. Biophys. J., 76 (1999) 3158–3166.

[35] M. G. Miguel, A. A.C.C. Pais, R. S. Dias, C. Leal, M. Rosa, B. Lindman, DNA–cationic amphiphile interactions, Colloids and Surfaces A: Physicochem. Eng. Aspects, 228 (2003) 43-55.

[36] P.J.C. Lin, Y.K. Tam, P.R. Cullis, Development and clinical applications of siRNA-encapsulated lipid nanoparticles in cancer, Clinical Lipidology, 9 (2014) 317-331.

[37] J. Gustafsson, G. Arvidson, G. Karlsson, M. Almgren, Complexes between cationic liposomes and DNA vizualized by cryo-TEM. Biochim. Biophys. Acta, 1235 (1995) 305-312.

[38] B. Angelov, A. Angelova, S.K. Filippov, G. Karlsson, N. Terrill, S. Lesieur, P. Štěpánek, SAXS study of sterically stabilized lipid nanocarriers functionalized by DNA, Journal of Physics: Conference Series, 351 (2012) 012004 (1-9).

[39] P.C.A. Barreleiro, R.P. May, B. Lindman, Mechanism of formation of DNA–cationic vesicle complexes. Faraday Discuss., 122 (2002) 191–201.

[40] S. Chen, Y.Y. Tam, P. J. Lin, A.K. Leung, Y.K. Tam, P.R. Cullis, Development of lipid nanoparticle formulations of siRNA for hepatocyte gene silencing following subcutaneous administration. Journal of Controlled Release, 196 (2014) 106-112.

[41] Y. Suzuki, K. Hyodo, Y. Tanaka, H. Ishihara. siRNA-lipid nanoparticles with long-term storage stability facilitate potent gene-silencing in vivo. Journal of Controlled Release, 220 (2015) 44-50.

[42] D. Chen, K.T. Love, Y. Chen, A.A. Eltoukhy, C. Kastrup, G. Sahay, A. Jeon, Y. Dong, K.A. Whitehead, D.G. Anderson, Rapid discovery of potent siRNA-containing lipid nanoparticles enabled by controlled microfluidic formulation. J. Am. Chem. Soc., 134, (2012) 6948−6951.

[43] H. Matsui, Y. Sato, H. Hatakeyama, H. Akita, H. Harashima, Size-dependent specific targeting and efficient gene silencing in peritoneal macrophages using a pH-sensitive cationic liposomal siRNA carrier, International Journal of Pharmaceutics, 495 (2015) 171-178.

[44] M.J. Hope, Enhancing siRNA delivery by employing lipid nanoparticles. Therapeutic Delivery, 5 (2014) 663-673.

[45] B. Ma, S. Zhang, H. Jiang, B. Zhao, H. Lv, Lipoplex morphologies and their influences on transfection efficiency in gene delivery, Journal of Controlled Release, 123 (2007) 184–194.

[46] J.P. Neves Silva, A.C.N. Oliveira, M.P.P.A. Casal, A.C. Gomes, P.J.G. Coutinho, O.P. Coutinho, M.E.C.D. Real Oliveira, Monoolein-based lipoplexes as non-viral vectors for transfection of mammalian cells, Biochimica et Biophysica Acta, 1808 (2011) 2440–2449.

[47] V.I. Martín, R.R. de la Haba, A. Ventosa, E. Congiu, J.J. Ortega-Calvo, M.L. Moyá, Colloidal and biological properties of cationic single-chain and dimeric surfactants, Colloids Surf. B: Biointerfaces, 114 (2014) 247–254.

[48] S. Mochizuki, N. Kanegae, K. Nishina, Y. Kamikawa, K. Koiwai, H. Masunaga, K. Sakurai, The role of the helper lipid dioleoylphosphatidylethanolamine (DOPE) for DNA transfection cooperating with a cationic lipid bearing ethylenediamine, Biochimica et Biophysica Acta - Biomembranes, 1828 (2013) 412-418.

[49] M. Cano−Sarabia, A. Angelova, N. Ventosa, S. Lesieur, Cholesterol induced CTAB micelle-to-vesicle phase transitions. J Colloid Interface Sci., 350 (2010) 10−15.

[50] A. Yaghmur, B. Sartori, M. Rappolt, The role of calcium in membrane condensation and spontaneous curvature variations in model lipidic systems, Physical Chemistry Chemical Physics, 13 (2011) 3115-3125.

[51] Z. Almshergi, S. Hyde, M. Ramachandran, Y. Deng, Cubic membranes: a structure-based design for DNA uptake. J. R. Soc. Interface, 5 (2008) 1023-1029.

[52] D. McLoughlin, M. Imperor-Clerc, D. Langevin, A new cubic phase containing DNA and surfactant. ChemPhysChem, 5 (2004) 1619-1629.

[53] I. Koltover, T. Salditt, J.O. Rädler, C.R. Safinya, Complexes related to DNA release and delivery an inverted hexagonal phase of cationic liposome-DNA, Science, 281 (1998) 78-81.

[54] J.O. Rädler, I. Koltover, T. Salditt, C.R. Safinya,, Structure of DNA-cationic liposome complexes: DNA intercalation in multilamellar membranes in distinct interhelical packing regimes, Science, 275 (1997) 810-814.

[55] E. Nazaruk, M. Szleĭzak, E. Górecka, R. Bilewicz, Y.M. Osornio, P. Uebelhart, E.M. Landau, Design and assembly of pH-sensitive lipidic cubic phase matrices for drug release, Langmuir, 30 (2014) 1383-1390.

[56] A. Zabara, R. Mezzenga, Controlling molecular transport and sustained drug release in lipid-based liquid crystalline mesophases, Journal of Controlled Release, 188 (2014) 31-43.

[57] A.H. Nagahara, D.A. Merrill, G. Coppola, S. Tsukada, B.E. Schroeder, G.M. Shaked, L. Wang, A. Blesch, A. Kim, JM Conner, E. Rockenstein, M.V. Chao, E.H. Koo, D. Geschwind, E. Masliah, A.A. Chiba, M.H. Tuszynski, Neuroprotective effects of brain-derived neurotrophic factor in rodent and primate models of Alzheimer's disease, Nat Med., 15 (2009) 331-337.

[58] J. Barauskas, C. Cervin, M. Jankunec, M. Spandyreva, K. Ribokaite, F. Tiberg, M. Johnsson, Interactions of lipid-based liquid crystalline nanoparticles with model and cell membranes, Int. J. Pharm., 391 (2010) 284−291.

[59] A.I.I. Tyler, H.M.G. Barriga, E.S. Parsons, N.L.C. McCarthy, O. Ces, R.V. Law, J.M. Seddon, N.J. Brooks, Electrostatic swelling of bicontinuous cubic lipid phases, Soft Matter, 11 (2015) 3279-3286.

[60] V.I. Petrenko, M.V. Avdeev, V.M. Garamus, L.A. Bulavin, V.L. Aksenov, L. Rosta, Micelle formation in aqueous solutions of dodecylbenzene sulfonic acid studied by small-angle neutron scattering, Colloids and Surfaces A: Physicochem. Eng. Aspects, 369 (2010) 160–164.

[61] V. I. Petrenko, V. L. Aksenov, M. V. Avdeev, L. A. Bulavin, L. Rosta, L. Vekas, V. M. Garamus, R. Willumeit, Analysis of the structure of aqueous ferrofluids by the small-angle neutron scattering method, Physics of the Solid State, 52 (2010) 974–978.

[62] D.B. Warren, M.U. Anby, A. Hawley, B.J. Boyd, Real time evolution of liquid crystalline nanostructure during the digestion of formulation lipids using synchrotron small-angle X-ray scattering, Langmuir, 27 (2011) 9528-9534.

[63] A. Angelova, B. Angelov, R. Mutafchieva, S. Lesieur, Biocompatible mesoporous and soft nanoarchitectures. J Inorg Organomet Polym., 25 (2015) 214–232.

[64] A. Angelova, B. Angelov, M. Drechsler, S. Lesieur, Neurotrophin delivery using nanotechnology, Drug Discovery Today, 18 (2013) 1263-1271.

[65] B. Angelov, A. Angelova, M. Drechsler, V. M. Garamus, R. Mutafchieva, S. Lesieur, Identification of large channels in cationic PEGylated cubosome nanoparticles by synchrotron radiation SAXS and Cryo-TEM imaging, Soft Matter, 11 (2015) 3686-3692.

[66] A. Angelova, C. Fajolles, C. Hocquelet, F. Djedaıni-Pilard, S. Lesieur, R. Cortesi, Physico-chemical investigation of asymmetrical peptidolipidyl-cyclodextrins, Journal of Colloid and Interface Science, 322 (2008) 304-314.

[67] A. Angelova, C. Ringard-Lefebvre and A. Baszkin, Drug-cyclodextrin association constants determined by surface tension and surface pressure measurements - I. Host-guest complexation of water soluble drugs by cyclodextrins: Polymyxin B-beta cyclodextrin system, J. Colloid Interface Sci., 212 (1999) 275-279.

[68] J. G. Petrov and A. Angelova, Interaction free energies in Langmuir-Blodgett multilayers of docosylammonium phosphate, Langmuir, 8 (1992) 3109-3115.

[69] A. Angelova, C. Ringard-Lefebvre and A. Baszkin, Drug-cyclodextrin association constants determined by surface tension and surface pressure measurements - II.

Sequestration of water insoluble drugs from the air-water interface: Retinol-beta cyclodextrin system, J. Colloid Interface Sci., 212 (1999) 280-285.

[70] A. Angelova, J. Reiche, R. Ionov, D. Janietz, L. Brehmer, Control of the structure of Langmuir-Blodgett films of a discotic liquid crystalline compound via the subphase composition and the adjacent molecular environment, Thin Solid Films, 242, (1994) 289-294.

[71] L. Zerkoune, S. Lesieur, J.-L. Putaux, L. Choisnard, A. Gèze,D. Wouessidjewe, B. Angelov, C. Vebert-Nardin, J. Doutch, A. Angelova, Mesoporous self-assembled nanoparticles of biotransesterified cyclodextrins and nonlamellar lipids as carriers of water-insoluble substances, Soft Matter, 12 (2016) 7539-7550.

[72] Y.Y. Chen, A. Angelova, B. Angelov, M. Drechsler, V.M. Garamus, R. Willumeit-Römer, A.H. Zou, Sterically stabilized spongosomes for multidrug delivery of anticancer nanomedicines. J Mater Chem B, 3 (2015) 7734-7744.

[73] L. Zerkoune, A. Angelova and S. Lesieur, Nano-assemblies of modified cyclodextrins and their complexes with guest molecules: Incorporation in nanostructured membranes and amphiphile nanoarchitectonics design, Nanomaterials, 4 (2014) 741-765.

Figure captions

Figure 1. Synchrotron SAXS patterns of aqueous dispersions of self-assembled lipid MO/EPC14/DOPE-PEG_{2000} carriers at varying molar percentages of the cationic component (15, 20 and 25 mol% EPC14) before (a) and after uptake and complexation (b) with plasmid DNA (pBDNF). The concentration of the PEGylated lipid DOPE-PEG_{2000} in the mixed assemblies was kept constant (3 mol%). The arrow in (a) indicates the position of a weak peak of an inverted hexagonal structure. The Bragg peaks of an inverted hexagonal lattice are indexed in (b).

Figure 2. Synchrotron SAXS patterns of aqueous dispersions of self-assembled lipid MO/CTAB/DOPE-PEG_{2000} carriers at varying molar percentages of cationic component (15, 20 and 25 mol% CTAB) before (a) and after uptake and complexation (b) with plasmid DNA (pBDNF). The concentration of the PEGylated lipid DOPE-PEG_{2000} in the mixed assemblies was kept constant (2 mol%). The arrow in (a) indicates the position of a weak peak of an inverted hexagonal structure. The Bragg peaks of two coexisting inverted hexagonal structures are indexed in (b).

Figure 3. Comparison of SAXS patterns of MO/EPC14/DOPE-PEG_{2000} and MO/CTAB/DOPE-PEG_{2000} nanocarriers and of the corresponding lipoplexes with pDNA (MO-EPC14-pDNA and MO-CTAB-pDNA) formed at constant positive charge (20 mol% cationic lipid content). The concentration of the DOPE-PEG_{2000} lipid in the mixed assemblies is 3 mol% in the case of EPC-containing carriers (a) and 2 mol% for CTAB-containing nanocarriers (b).

Figure 4. Cryogenic transmission electron microscopy (Cryo-TEM) images showing stages of formation of self-assembled lipoplex nanostructures of liquid crystalline organization: (a,b) nanoparticles with onion lamellar packing; (c,d) intermediates of inverted hexagonal packing, and (e) hexosome carriers with long range order of inverted hexagonal structure. The bar corresponds to 100 nm.